RSC Advances

ROYAL SOCIETY
OF CHEMISTRY

www.rsc.org/advances

RSC Advances

PAPER

Critical role of silk fibroin secondary structure on the dielectric performances of organic thin-film transistors

Min Hong Park,[a†] Junhyung Kim,[b†] Seung Chul Lee,[b] Se Youn Cho,[a] Na Rae Kim,[a] Boseok Kang,[c] Eunjoo Song,[c] Kilwon Cho,[c] Hyoung-Joon Jin,[a,]* and Wi Hyoung Lee[b,]*

Silk fibroin (SF) is being considered as an emerging class of dielectric material in electronics, such as organic thin-film transistors (OTFTs). SF has several advantageous properties, including high transparency, flexibility, and solution-processability. In this study, we investigated the effects of processing solvent and post-treatment on the surface properties and structural development of SF films, which were used in gate-dielectric of OTFTs. The SF films cast from aqueous solution exhibited an amorphous structure with random coil conformations, leading to poor dielectric properties that were inadequate for developing OTFTs. In contrast, the use of formic acid solution and sequential methanol vapor treatment after film casting induced smoother SF surface. Moreover, its crystallinity also improved dramatically. Furthermore, the SF films cast from formic acid solution and treated with methanol vapor were capable of growth of highly ordered organic semiconductor thin films deposited on these films. As a result, pentacene TFTs fabricated with the SF films showed high performance and stable operation with nearly zero turn-on voltage, negligible hysteresis, and high bias stability. This indicates a strong correlation between the structure of SF film and dielectric performances of OTFTs. We believe that our study would be useful in designing silk materials, which are highly compatible with human interface and other biological environments.

1. Introduction

Scientists have focused their attention on developing different techniques that fabricate soft electronic devices, which are light, flexible, and stretchable.[1-2] As a result, the conventionally hard and rigid electronics are now being replaced by polymer- based electronics on a commercial scale. Presently, dielectric components in organic thin-film transistors (OTFTs) and organic semiconductors are promising candidates in the field of soft and portable electronics. Several research studies have tried to develop organic semiconductors that exhibit excellent electrical capacity.[3-10] However, it is still quite challenging to construct a suitable gate dielectric material, having high dielectric strength and solution processibility.[11-13]

Among the diverse protein materials present in nature, silk fibroin (SF), which is extracted from *Bombyx mori* (*B. mori*) silkworm cocoons, is the most abundant protein. Since ancient times, clothing fabrics of high quality have been manufactured using SF as the raw material. This is because SF has several superior properties, such as lightness, fineness, a pleasant feel, and a unique luster.[14-16] In recent years, there have been rapid developments in manufacturing technology employed for synthesizing silk clothing. Moreover, with a growing concern for environmental degradation, researchers have been trying diligently to employ SF in various research fields, including photonics and electronics.[17-19] In particular, SF films have been used in the construction of gate dielectric materials of OTFT because these films have several advantageous features, such as solution-processability, flexibility, and optical transparency (ca.

> 90%). Moreover, SF films offer great resistance to organic solvents.[17, 20-22] Typically, SF solution is prepared from an aqueous solution; spin-casting or dip-coating of this solution leads to the SF films, having a thickness of several hundred nanometers. Wang *et al*. have employed 420 nm thick SF film (capacitance of 30 nF/cm^2) as the gate dielectric material in the fabrication of a pentacene OTFT, which exhibits high field-effect mobility and at a low operating voltage.[17] Shi *et al*. have developed a poly(3-hexylthiophene) based OTFT using a 337 nm thick SF film (capacitance of 10.8 nF/cm^2) as the gate-dielectric material; this OTFT operates in devices driven by low voltage.[20]

Compared with other conventional polymers, such as polystyrene ($\approx$2.5), poly (methyl methacrylate) (PMMA, $\approx$3.5), and poly(vinyl phenol) (PVP, $\approx$4.5), SF has a relatively high dielectric constant ($\approx$7).[12] However, in previous studies, researchers could not decipher low voltage operation using thick SF films with low capacitances. One of the possible reasons is that SF film contains ionic impurities during the preparation of SF aqueous solution. But, these impurities can affect electrical properties. Tsai *et al*. have reported that field-effect mobility of n-type C_{60} OTFT with SF gate-dielectric increases by about three orders of magnitude when OTFT is exposed to ambient air.[22] They have proposed that sericin, an amino acid residue, can react with water in ambient air, inducing charged ions in SF gate dielectric. Subsequently, these charged ions form an electrical double-layer while boosting source-drain current under gate-bias. In this regard, it is necessary to exactly determine electrical properties in well-

controlled condition. Thus, we need to examine intrinsic properties of OTFTs with SF gate-dielectric.

When a polymeric material is used as a gate-dielectric in OTFTs, the chemical and physical properties of the polymer affect the insulating ability of OTFTs. The most common insulating polymers, such as polystyrene and poly(methyl methacrylate) exhibit low breakdown strength. Therefore, cross-linked polymers such as poly(vinyl phenol) and poly (vinyl alcohol) are preferred for constructing gate-dielectric.[23-25] Cross-linking agent can react with the functional groups in these polymers, forming network structures with high breakdown strength and solvent resistance. Alternatively, a network polymer film can be fabricated by executing a self-crosslinking process under heat or UV light.[26] Interestingly, recurrent glycine and alanine amino acids in SF films induce hydrogen bonding, which encourages the formation of secondary structures, such as antiparallel β-sheet. This structure is quite robust and stable in the presence of typical organic solvents because a cross-linked structure develops due to hydrogen bonding. Recently, Dickerson *et al.* have reported that the dielectric breakdown strength of SF dielectric is closely related to the extent of β-sheet crystals.[27] Thus, it is very interesting to examine how crystalline structure of SF film affects electrical properties of OTFTs, which are based on SF dielectric. We noticed that crystalline structure of SF film can be changed either by adopting different solvents that dissolve SF molecules or by implementing post-treatment procedure on SF film. In addition, surface properties, such as roughness and free energy can also be controlled using different processing solvents and post-treatment procedures. These surface properties ultimately determine growth characteristics and molecular ordering of organic semiconductors, thereby affecting the transport of charge carriers at the interface between organic semiconductor and SF dielectric.

In this study, SF films have been fabricated using two different solvents: water and formic acid. These solvents were used for fixing the final thickness of SF films. Post-treatment procedure using methanol vapor treatment was optionally applied on spin-cast SF films to increase crystallinity. We examined how the processing solvent and post-treatment procedure had an impact on the surface properties and structural development of SF films. For this purpose, we used various analytical techniques, including atomic force microscopy (AFM), contact angle measurement, Fourier transform infrared (FT-IR) spectroscopy, and two-dimensional grazing-incidence X-ray diffraction (2D-GIXRD). Then, we examined insulating properties of SF films by measuring current-voltage characteristics of metal-insulator-metal (MIM) devices. Finally, we fabricated pentacene OTFTs using various SF films, and we measured device performances in vacuum to compare intrinsic properties of OTFTs with SF gate-dielectric.

2. Experimental details

2.1 Materials

Cocoons of *B. mori* silkworms were purchased from the Uljin Farm, South Korea. To extract glue-like sericins and other impurities, we boiled these cocoons for 30 min in an aqueous solution containing 0.02 M Na_2CO_3 (99% purity; OCI Co., Korea). After washing several times with deionized (DI) water, SF, the resultant fibrous protein, was dried at room temperature for three days. The aqueous solutions of regenerated SF were prepared, as described elsewhere.[28] Briefly, degummed SF was dissolved in an aqueous solution of 9.3 M LiBr (99% purity; Sigma-Aldrich, USA) at 60 °C. The dissolution process was

carried out for six hours. In DI water, the SF solution was dialysed for 2 days using a Slide-a-Lyzer dialysis cassette (MWCO 3500, Pierce, USA). Thereafter, the SF solution was centrifuged at 9500 rpm for 30 min. The final concentration of SF in the aqueous solution was approximately 8 wt%. Before preparing the solution of SF in formic acid, the aqueous solution of SF was frozen in liquid nitrogen and subjected to lyophilisation at –50 ºC and 0.045 mbar for 72 hours. The resultant cylindrical SF sponge was dissolved in formic acid (98% purity; Junsei Chemical Co. Japan) till it attained a mass fraction of 5 wt%.

2.2 Fabrication of SF thin films

A simple spin-casting method was used to fabricate thin SF films on a silicon wafer, which was previously cleaned by immersing it in boiling acetone for 30 min and subjecting it to UV treatment for 30 min subsequently. Approximately 200 μL of two different SF solutions were deposited on the top of a silicon wafer by spin-coating with a speed of 7000 rpm. Regardless of the SF solution, the thickness of the resultant film was around 400 nm. Thereafter, SFW and SFF were respectively used to denote the thin SF films prepared using aqueous and formic acid solution of SF. These thin SF films were treated with a 90:10 (v/v) methanol/water vapor, which is a well-known method to develop a crystalline structure of SF. The resultant thin SF films were denoted as SFW-Me and SFF-Me.

2.3 Device fabrication

MIM devices and bottom-gate/top-contact OTFT devices were fabricated (Figure 1). In this process, MIM devices were fabricated by evaporating gold electrodes on thin SF films using a shadow mask. For constructing OTFT devices, a 50 nm thick pentacene layer was deposited by thermal evaporation at room temperature on thin SF films. Then, using a shadow mask on pentacene films, we evaporated source–drain electrodes with 60 nm thick gold coating. The channel length and width of fabricated OTFTs were 50 μm and 300 μm, respectively.

2.4 Characterization

We examined the surface morphologies of thin SF films and pentacene films using atomic force microscopy (AFM, SPA400, Seiko Ins., Japan). Fourier transform infrared spectroscopy (FT-IR, Bruker, VERTEX 80V, Germany) was used to examine β-sheet crystalline structures of thin SF films. On the other hand, two-dimensional grazing-incidence X-ray diffraction (2D-GIXRD, 9A beamline in Pohang Accelerator Laboratory of Korea) was used to detect crystalline structures of both thin SF films (thickness of ~ 400 nm) and pentacene films (thickness of approximately 20 nm). The surface polarity of thin SF films was determined from contact angle measurements (N = 5, average ± standard deviation). The capacitances of silk films were measured using an Agilent E4980A Precision LCR meter, while current-voltage characteristics of OTFT devices were measured using a Keithley 4200-SCS Source Measure Unit under vacuum conditions.
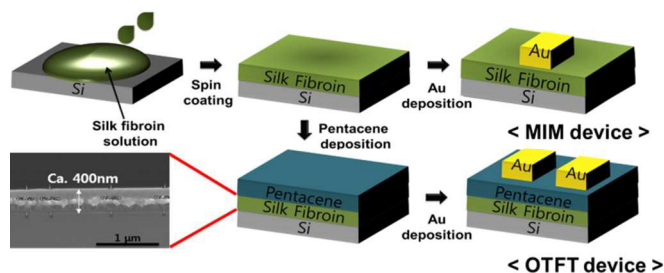
Figure 1. Schematics of MIM device, OTFT device, and FE-SEM image of SF thin film prepared using formic acid as a solvent.
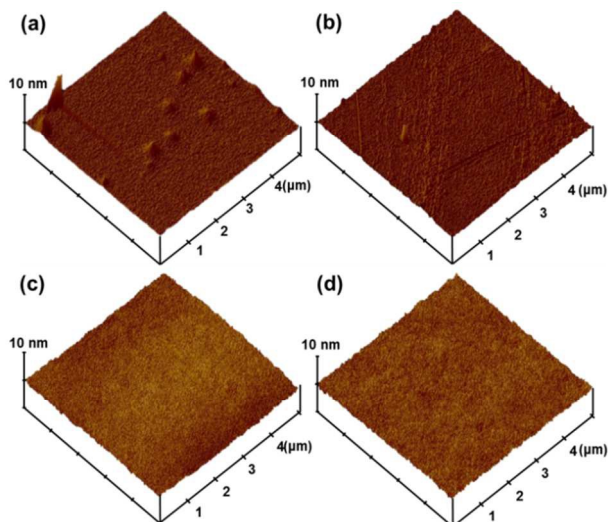
3. Results and discussion

Figure 2. AFM topographies of SF thin films prepared with different methods: (a) SFW, (b) SFW-Me, (c) SFF, and (d) SFF-Me.

We determined the surface roughness of SF dielectric films on Si substrates by AFM (**Figure 2**). These SF dielectric films were developed on Si substrates using two different solutions. The root mean square (rms) values of 2.3 and 0.7 nm represented the surface roughness of SF thin film of 5 μm × 5 μm area, which consisted of SFW and SFF, respectively. Although all the thin SF films were fabricated under the same spinning conditions, the thin SF film that was prepared using formic acid as a solvent exhibited significantly lower values of surface roughness as compared to that of thin SF film prepared using water. This result might be attributed to the different solvent evaporation rates of solvents used for constructing these SF films.[29-31] As solvents have different pressure, the film formation process of SF gets affected during solvent evaporation. In particular, a low vapor pressure of formic acid induces slow solvent evaporation, which assists the formation of a smoother surface in a spin-cast thin SF film. In addition, after post-treatment with methanol vapor, SF dielectric layers exhibit slightly lower rms values of 1.9, and 0.4 nm, which represent surface roughness of SFW-Me, and SFF-Me, respectively. This result indicates that solvent vapor can efficiently reduce the roughness of SF film.
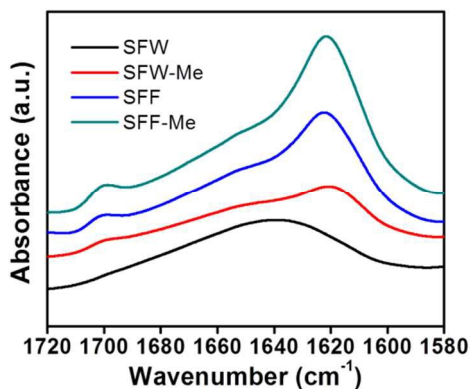

Figure 3. FT-IR spectra of SF thin films prepared with different methods.

Crystalline structures of SF thin films depend on processing solvents and post-treatment procedures. These crystalline structures were investigated by FT-IR and 2D-GIXRD (**Figure 3 and 4**). The amide group of SF has characteristic vibrational modes (amide modes), which are sensitive to protein conformation.[32] In particular, amide I (1700–1600 cm^{-1}) region is commonly used to determine the secondary structure of SF. The absorption bands appear in the range of 1610–1630 cm^{-1}; an absorption peak also appears around 1700 cm^{-1}. These are characteristic peaks representing the β-sheet crystalline structure, whereas broad and indistinct amide I bands represent the random coil structure.[33] As shown in **Figure 3**, SFW showed broad absorption peaks at 1640 cm^{-1}, corresponding to the random coil conformation. Following treatment with methanol vapor, the amide I bands of SFW-Me showed peaks at 1622 and 1700 cm^{-1}, indicating structural changes in the β-sheet crystalline structure. Furthermore, strong absorption peaks corresponding to β-sheet crystalline structure were exhibited by SFF. When SFF was treated with methanol vapor, there was increase in intensity of these peaks. Formic acids strongly interact with the polar moiety of amino acids in SF molecules, which leads to a closer packing of amino acids with the nonpolar side groups.[34] When formic acid evaporates slowly, these amino acids along with nonpolar side groups tend to crystallize into β-sheet crystalline structure. On the other hand, water molecules interact any kinds of amino acids in SF and thus SF exists in a loosely packed structure. Accordingly, evaporation of water results in a random coil conformation in the solid state of SF film.
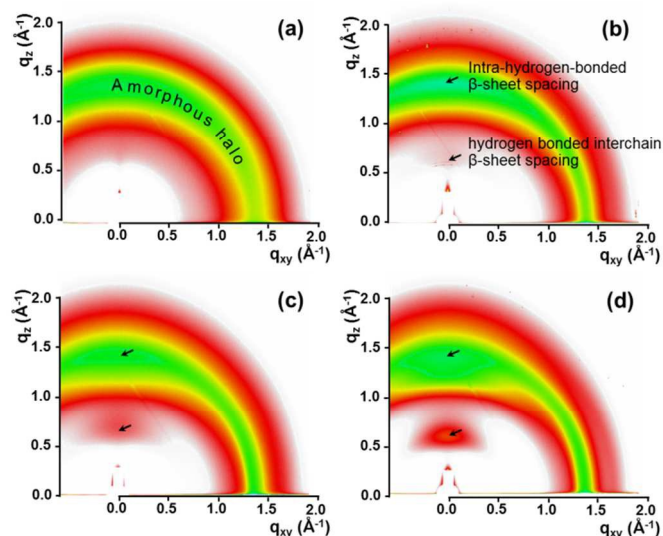

Figure 4. GI-XRD patterns of SF thin films prepared with different methods. (a) SFW, (b) SFW-Me, (c) SFF, and (d) SFF-Me.

Table 1. Water contact angle of silk fibroin thin films prepared from different methods

	Silk fibroin thin films			
	SFW	SFW-Me	SFF	SFF-Me
Contact angle (degree)	46.4 ± 4.1	58.1 ± 0.5	65.9 ± 1.8	72.1 ± 1.3

The 2D-GIXRD results agree well with the FTIR analysis. As shown in **Figure 4(a)**, 2D-GIXRD pattern of SFW includes a broad and diffused peak at q = ~ 1.4 A^{-1}. This peak is attributed to the amorphous structure of SF with random coil conformations. However, in the GI-XRD pattern of SFW-Me, broad peak become narrower, and peak center shifts slightly to a higher q_z value (~ 1.46 A^{-1}). In addition, there is a new peak at q_z = ~ 0.64 A^{-1}, corresponding to the interchain β-sheet spacing between hydrogen bonds.[35] When formic acid was used as a solvent, a peak at q_z = ~ 0.64 A^{-1} was detected even before annealing methanol vapor (**Figure 4(c)**). This result also indicates how formic acid can effectively crystallize SF into β-sheet crystalline structure. In the GI-XRD pattern of SFF-Me, the appearance of distinctive peaks at ~ 0.64 and ~ 1.46 A^{-1} prove the dominance of β-sheet crystalline structures in SFF-Me (**Figure 4(d)**).[35] The surface polarity of SF thin films was examined by measuring the contact angle and summarizing it in **Table 1**. The contact angle of SFW, SFW-Me, SFF, and SFF-Me was 46.4 ± 4.1, 58.1 ± 0.5, 66.9 ± 1.8, and 72.1 ± 1.3°, respectively. This can be explained by considering the crystallization induced by structural changes in SF film. **Figure 5** shows a schematic diagram, indicating a change in the structure of silk gate-dielectric by crystallization. In an amorphous state, polar side groups are randomly oriented in amino acids, contributing to a high surface energy in SFW. During crystallization, hydrogen bonds grab the polar side groups into the bulk dielectric film, leading to the formation of a stable β-sheet structure (**Figure 5** right). Thus, the surface of SF thin film became hydrophobic with an increase in β-sheet structure. Considering the results of FTIR, GI-XRD, and contact angle, the amount of β-sheet crystalline structure can be compared in the following order: SFF-Me > SFF > SFW-Me > SFW.
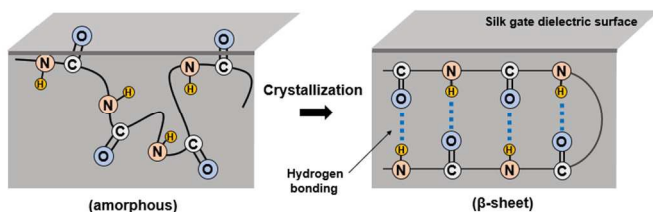

Figure 5. Schematic diagram showing a change in the structure of SF film by crystallization.

To evaluate the insulating properties of SF dielectric, we determined the dielectric break-down strength by measuring current-voltage characteristics of MIM devices (**Figure 6**). At around 4 V, SFW showed an early breakdown, corresponding to a break-down field of 0.07 MV/cm (**Figure 6a**). Because SFW exhibits an amorphous or random coil conformation, it is very weak against an applied electric field. Contact angle measurements indicate that SFW is vulnerable to water and other organic solvents. This limits the use of SF film from an aqueous solution in a dielectric layer, which needs to be robust enough to create a dense layer of high break-down strength. In SFW-Me, the dielectric break-down voltage increased slightly. However, SFW-Me still showed an early break-down owing to low crystallinity. It is noteworthy that the dielectric breakdown strength increased remarkably in SFF. Furthermore, SFF did not show a breakdown until 80V, which corresponded to a breakdown field of over 2.0 MV/cm. Because the thicknesses of dielectric films are nearly the same (ca. 400 nm), the huge differences in breakdown behaviors of dielectric are associated with the structures of silk films. The use of formic acid

facilitates the formation of β-sheet structure, which is stabilized by physical cross-linking with hydrogen bonds. Thus, with a high percentage of β-sheet structure, SFF can endure high breakdown field. Furthermore, the current density in SFF-Me decreases to a greater extent in the same electric field. This indicates that SFF-Me is the most stable among the four silk samples. This statement was further corroborated by examining weight changes of SFF-Me in various solvents (**Table 2**). When SFF-Me was dipped into five types of organic solvents, there was practically no weight loss until 4 weeks. This high stability is due to the existence of β-sheet structure, as shown in **Figure 5**. Note that, β-sheet crystalline structure is one of the most stable secondary structures in nature, which are assembled by numerous inter-chain hydrogen bonds between adjacent peptide blocks.
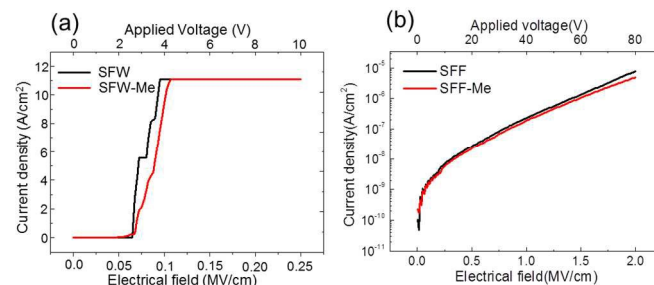

Figure 6. Dielectric break-down strength of SF thin films: (a) SFW, SFW-Me and (b) SFF, SFF-Me.

Table 2. Weight changes of SFF-Me in various solvents during four weeks

Solvent	Initial	After 2 weeks	After 4 weeks
Chloroform	10.4 mg	10.4 mg	10.3 mg
Cyclohexene	9.7 mg	9.7 mg	9.7 mg
DMF	10.6 mg	10.6 mg	10.6 mg
THF	6.5 mg	6.5 mg	6.5 mg
Toluene	10.0 mg	9.9 mg	9.8 mg

To determine the possible utility of SF films in the dielectric layer of OTFTs, we deposited pentacene on SFF and SFF-Me. **Figure 7** shows AFM images of 50 nm thick pentacene films on two different silk dielectrics. Because SFW and SFW-Me showed an early dielectric breakdown at around 4 V, we excluded these SF films while carrying out the characterization of pentacene morphology of OTFTs. Both pentacene films on SFF and SFF-Me exhibited a terraced growth of pentacene grains. Thus, grain sizes of pentacene films were nearly the same. Although the roughness of SFF (~0.7 nm) or SFF-Me (~0.4 nm) was slightly higher than SiO_2 dielectric (~0.2 nm), the growth of pentacene grain was not affected significantly. Moreover, the grain size of pentacene on SFF or SFF-Me is larger than that of pentacene on SiO_2 dielectric (see **Figure S1** in Supporting information for AFM image of pentacene on SiO_2).

To further investigate molecular ordering within pentacene grains, we obtained 2D-GIXRD patterns of pentacene films on SFF and SFF-Me (**Figure 8**). SFF displayed intense (00l) diffractions in the thin-film crystalline phase (indicated by (00l)$_T$) along with q_z. In addition, we also observed small peaks corresponding to the bulk crystalline phase (indicated by arrow and (00l)$_B$), which is slightly titled along q_z. In accordance with

the diffraction patterns along q_z, vertically aligned intense in-plane reflections, {1, ±1}, {0, 2} in the thin film phase (indicated by {1, ±1}$_T$, {0, 2}$_T$) were also observed. These Bragg rod reflections indicate that pentacene adopted highly ordered multi-layered structures.[36] SFF-Me displayed similar 2D-GIXRD patterns; however, $(00l)_B$ is weaker than that of SFF. This result implies that crystalline homogeneity in SFF-Me is better than SFF. Because surface energy of SFF-Me is slightly lower that of SFF, hydrophobic SFF-Me surface facilitates homogeneous growth of pentacene crystals with thin-film crystalline phase.[37] In contrast, pentacene film on SiO₂ dielectric shows larger amounts of $(00l)_B$, and {1, ±1}, {0, 2} Bragg rod reflections were tilted greatly (see **Figure S2** in Supporting information). This indicates that SiO₂ surface yielded higher amount of mismatch in pentacene crystals.
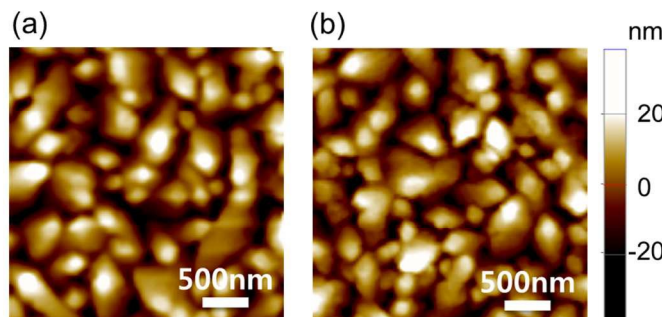

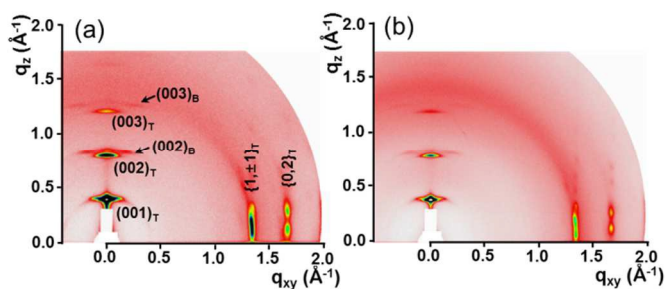**Figure 7**. AFM images of pentacene films on (a) SFF and (b) SFF-Me.

Figure 8. 2D-GIXRD patterns of pentacene films on (a) SFF and (b) SFF-Me.

After depositing Au source/drain electrodes, we examined the electrical properties of pentacene TFTs with SFF, SFF-Me, and SiO₂ dielectric. Transfer characteristics were measured by sweeping gate bias in dual directions under vacuum (**Figure 9 and Figure S3** in Supporting information). Besides exhibiting high on-current, TFTs with SFF-Me show nearly zero turn-on voltage (V_{on}) and hysteresis in dual sweeps. On the other hand, TFTs with SFF display large V_{on} and clock-wise hysteresis, a phenomenon which is common in cross-linked gate-dielectric with residual hydroxyl groups.[38-40] SFF can contain free CO and NH groups, which are not restricted to inter-chain hydrogen bonding in β-sheet structure. Under negative gate-bias, these mobile groups increase dipole of the gate-dielectric, inducing slow polarization. This ultimately causes large V_{on} and clock-wise hysteresis. The slow polarization observed in TFTs with SFF does not occur in TFTs with SFF-Me because CO and NH groups are strongly restricted by hydrogen bonding in β-sheet structure. Thus, TFTs with SFF show nearly zero V_{on} and hysteresis. In TFTs with SiO₂, however, counter-clockwise hysteresis was observed in dual sweeps (see **Figure S3** in Supporting information). This behavior can be explained by

considering charge trappings at the surface of SiO₂.[41] It is known that silanol (Si-OH) groups in SiO₂ surface trigger the trappings of electron. These electron trappings cause a decrease in hole by carrying out reverse sweep.[42] For performing quantitative analysis of hysteresis, we calculated maximum gate voltage shift ($\Delta V^{max}_{hysteresis}$) in dual sweeps. In TFTs with SiO₂, 22.3V was obtained while in TFTs with SFF-Me, this value is only 1.7 V. This proves the outstanding stability of TFTs in SFF-Me.
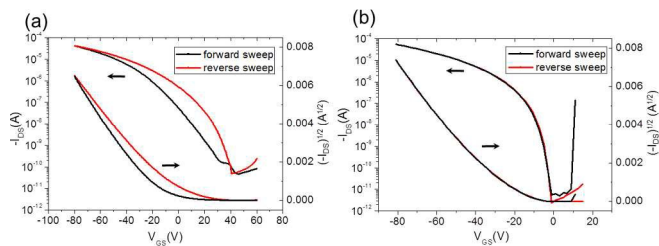

Figure 9. Transfer characteristics of pentacene TFTs with (a) SFF and (b) SFF-Me.

Field-effect mobility (μ) was calculated by equation (1) in the saturation regime:

$$I_{DS} = \frac{W C_i}{2 L} \mu (V_{GS} - V_T)^2 \tag{1}$$

where I_{DS} is the drain current; V_{GS} is the gate voltage; V_T is threshold voltage; C_i is areal capacitance; and W and L are the channel width (300 μm) and length (50 μm), respectively. Areal capacitances of SFF and SFF-Me were calculated by measuring capacitances in the MIM devices. (See **Figure S4** in supporting information). C_i of SFF and SFF-Me were 14.5 nF/cm² and 14.0 nF/cm² at 100 kHz, corresponding to dielectric constant of 7.1 and 6.9, respectively. Compared to SFF, the areal capacitance (or dielectric constant) of SFF-Me is relatively low, which might be related with the crystallization of silk film. Because polar groups in peptide blocks are strongly restricted by hydrogen bonds, polarization effect is weakened. The μ values of 0.38 and 0.43 cm²V⁻¹ s⁻¹ were obtained by pentacene TFTs using SFF and SFF-Me, respectively (see **Table 3** for summary of electrical properties). Pentacene film on SFF-Me yielded higher crystalline homogeneity than on SFF. This slightly increases field-effect mobility. On the other hand, we found that μ of pentacene TFTs with SiO₂ dielectric was 0.14 cm² V⁻¹ s⁻¹. The relatively low field-effect mobility is due to the combined effects of small grain size and a high amount of mismatch in pentacene crystals of SiO₂. Note that, crystals with bulk phase in this pentacene film induce crystalline mismatch with crystals in the thin-film phase, resulting in the scattering of charge carriers.

Table 3. Electrical properties of OTFTs based on silk fibroin thin films

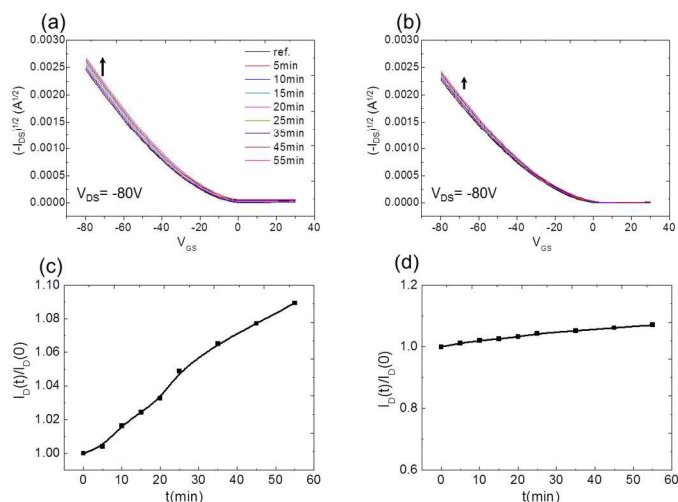|	Mobility (cm²/Vs)	ON/OFF current ratio	V_{on} (V)	$\Delta V^{max}_{hysteresis}$ (V)
SFF	0.38 (±0.02)	~10⁶	31.9 (±3.9)	18.7 (±1.6)
SFF-Me	0.43 (±0.01)	~10⁸	-0.3 (±0.05)	1.7 (±0.3)
SiO₂	0.14 (±0.05)	~10⁸	0.5 (±0.1)	22.3 (±2.3)

Figure 10. Gate bias stabilities of pentacene TFTs with (a) SFF and (b) SFF-Me. Bias of $V_{GS} = -60$ V and $V_{DS} = -3$V were applied on the TFTs and transfer characteristics were measured at given time intervals. Extracted on-current changes from (a) and (b) were plotted in (c) and (d), respectively.

The electrical stability under continuous gate-bias is another important performance parameter to ensure long-term operation of TFTs in a display backplane.[43-45] **Figure 10** exhibits comparative plots of electrical stabilities of pentacene TFTs with SFF and SFF-Me under $V_{GS} = -60$ V and $V_{DS} = -3$V. Moreover, TFTs with SFF display a gradual increase of source-drain current (or positive threshold voltage shift) with bias stress time (**Figure 10 a, c**). This behavior corresponds well with clockwise hysteresis in Figure 9(a), and this behavior can be explained by slow polarization.[38-40] In particular, more hole carriers can be accumulated at the channel/SFF interface by remnant dipoles in SF film. In TFTs with SFF-Me, inter-chain hydrogen bonding in β-sheet structure tightly binds with the polar groups of peptide bonding, resulting in nearly unchanged electrical properties (See **Figure 10 b, d**). It is interesting to note that inter-chain hydrogen bonding is one kind of secondary bonding; however, it is strong enough to confine functional groups in peptide and to maintain secondary structure (i.e., β-sheet structure) against an electric field in the presence of organic solvent. In TFTs with SiO_2 dielectric, however, charge trapping at the pentacene/SiO_2 interface leads to current decay (or negative threshold shift) upon gate-bias stress (see **Figure S5** in supporting information). When pentacene TFTs were built on SFW and SFW-Me, we could not detect field-effect behaviors mainly due to a large leakage current across dielectric films. This explains the critical role of solvent and vapor treatment, which governs the structure and performance of SF gate-dielectric in OTFTs. The field-effect mobility of 0.43 cm^2 V^{-1} s^{-1} in pentacene TFTs with SFF-Me is relatively low compared to recent report that used SF film from aqueous solution as a gate-dielectric in OTFTs.[17] We speculate that they have high mobility due to the hydroscopic nature of SF film with low crystallinity.[22] Unlike their experiments, all the electrical measurements in our experiment have been conducted in vacuum. Thus, it can be said that the unusual hydroscopic nature of SF film was excluded, and intrinsic properties of SF gate-dielectric for OTFTs were studied. Especially, inter-chain hydrogen bonding in β-sheet structure plays a key role in both insulating properties of gate-dielectric and electrical properties of OTFTs, which are based on SF gate-dielectric.

4. Conclusions

In this study, we investigated surface, structural, and dielectric properties of SF thin films that were prepared using two different solvents: water and formic acid. SF thin film that was fabricated using formic acid (SFF) showed lower surface roughness due to slow evaporation of formic acid. Structural characterization revealed that β-sheet crystalline structure was preferentially formed in SFF. Furthermore, crystallization with post-treatment using methanol vapor (SFF-Me) led to an increase in the amount of β-sheet crystalline structure. This structure with inter-chain hydrogen bonding was advantageous for increasing the dielectric breakdown strength of SF film. SF film cast from water exhibited a low breakdown field of 0.07 MV/cm, while SF films cast from formic acid (SFF, SFF-Me) showed a breakdown field at over 2 MV/cm. Pentacene was deposited on SFF and SFF-Me, which have insulating properties that can be sufficiently used in TFTs. Morphological and structural characterizations revealed that pentacene films with larger grain and crystal homogeneities were observed on SFF and SFF-Me but the same features were not observed in SiO_2 dielectric. Interestingly, hysteresis behavior and gate bias stability of pentacene TFTs with SFF were completely opposite to those with SiO_2. These characteristics could be explained by slow polarization of residual functional groups of peptides, which are not coupled with inter-chain hydrogen bonding. Remarkably, pentacene TFTs with SFF-Me exhibited nearly zero V_{on}, negligible hysteresis, and high bias stability. These features can be attributed to inter-chain hydrogen bonding in β-sheet structure that is stable against electric field and organic solvent. Our work proves that the structure of SF film should be well controlled for obtaining suitable electrical properties of OTFTs in SF film, which is highly recommended for ensuring compatibility with human interface and other biological environments.

Notes and references

[a] Department of Polymer Science and Engineering, Inha University, Incheon 402-751, Korea
[b] Department of Organic and Nano System Engineering, Konkuk University, Seoul 143-772, Korea
[c] Department of Chemical Engineering, Pohang University of Science and Technology (POSTECH), Pohang 790-784, Korea

[†] M. H. Park and J. Kim contributed equally to this work.
*Corresponding author. Tel: +82-2-450-3468; Fax: +82-2-457-8895.
E-mail address: whlee78@konkuk.ac.kr (W. H. Lee), hjjin@inha.ac.kr (H.-J. Jin)

1   S. R. Forrest, *Nature,* 2004**, 428**, 911-918.

2   J. A. Rogers and Y. G. Huang, *P. Natl. Acad. Sci. USA* 2009**, 106**, 16889-16889.

3   H. Sirringhaus, *Adv. Mater.,* 2014**, 26**, 1319-1335.

4   L. Zhang, N. S. Colella, B. P. Cherniawski, S. C. Mannsfeld and A. L. Briseno, *ACS Appl. Mater. Inter.,* 2014**, 6**, 5327-5343.

5   A. Facchetti, *Mater Today,* 2007**, 10**, 28-37.

6   J. E. Anthony, A. Facchetti, M. Heeney, S. R. Marder and X. W. Zhan, *Adv. Mater.* 2010**, 22**, 3876-3892.

7   Y. N. Li, P. Sonar, L. Murphy and W. Hong, *Energ. Environ. Sci.,* 2013**, 6**, 1684-1710.

8   J. Li, Y. Zhao, H. S. Tan, Y. L. Guo, C. A. Di, G. Yu, Y. Q. Liu, M. Lin, S. H. Lim, Y. H. Zhou, H. B. Su and B. S. Ong, *Sci. Rep.-Uk,* 2012**, 2**, 754.

9   I. Kang, H. J. Yun, D. S. Chung, S. K. Kwon and Y. H. Kim, *J. Am. Chem. Soc.,* 2013**, 135**, 14896-14899.

10 S. Holliday, J. E. Donaghey and I. McCulloch, *Chem. Mater.,* 2014**, 26**, 647-663.

11 A. Facchetti, M. H. Yoon and T. J. Marks, *Adv. Mater.,* 2005**, 17**, 1705-1725.

12 J. Veres, S. Ogier, G. Lloyd and D. de Leeuw, *Chem. Mater.,* 2004**, 16**, 4543-4555.

13 H. Klauk, U. Zschieschang, J. Pflaum and M. Halik, *Nature* 2007**, 445**, 745-748.

14 J. M. Deitzel, J. Kleinmeyer, D. Harris and N. C. B. Tan, *Polymer* 2001**, 42**, 261-272.

15 G. H. Altman, R. L. Horan, H. H. Lu, J. Moreau, J. C. Richmond and D. L. Kaplan, *Biomaterials* 2002**, 23**, 4131-4141.

16 Z. Z. Shao and F. Vollrath, *Nature* 2002**, 418**, 741-741.

17 C. H. Wang, C. Y. Hsieh and J. C. Hwang, *Adv. Mater.*, 2011, **23**, 1630-1634.

18 E. Steven, V. Lebedev, E. Laukhina, C. Rovira, V. Laukhin, J. S. Brooks and J. Veciana, *Mater. Horizons*, 2014, **1**, 522-528.

19 S. T. Parker, P. Domachuk, J. Amsden, J. Bressner, J. A. Lewis, D. L. Kaplan and F. G. Omenetto, *Adv. Mater.*, 2009, **21**, 2411-2415.

20 L. L. Shi, X. J. Xu, M. C. Ma and L. D. Li, *Appl. Phys. Lett.*, 2014, **104**, 023302-023304.

21 R. Capelli, J. J. Amsden, G. Generali, S. Toffanin, V. Benfenati, M. Muccini, D. L. Kaplan, F. G. Omenetto and R. Zamboni, *Org. Electron.*, 2011, **12**, 1146-1151.

22 L. S. Tsai, J. C. Hwang, C. Y. Lee, Y. T. Lin, C. L. Tsai, T. H. Chang, Y. L. Chueh and H. F. Meng, *Appl. Phys. Lett.*, 2013, **103**, 233304-233306.

23 Z. N. Bao, V. Kuck, J. A. Rogers and M. A. Paczkowski, *Adv. Funct. Mater.*, 2002, **12**, 526-531.

24 Y. Jang, D. H. Kim, Y. D. Park, J. H. Cho, M. Hwang and K. W. Cho, *Appl. Phys. Lett.*, 2006, **88**, 072101-072103.

25 M. H. Yoon, H. Yan, A. Facchetti and T. J. Marks, *J. Am. Chem. Soc.*, 2005, **127**, 10388-10395.

26 J. Y. Jang, S. H. Kim, S. Nam, D. S. Chung, C. W. Yang, W. M. Yun, C. E. Park and J. B. Koo, *Appl. Phys. Lett.*, 2008, **92**, 143306-143308.

27 M. B. Dickerson, S. P. Fillery, H. Koerner, K. M. Singh, K. Martinick, L. F. Drummy, M. F. Durstock, R. A. Vaia, F. G. Omenetto, D. L. Kaplan and R. R. Naik, *Biomacromolecules*, 2013, **14**, 3509-3514.

28 H. J. Jin and D. L. Kaplan, *Nature*, 2003, **424**, 1057-1061.

29 W. H. Lee, D. Kwak, J. E. Anthony, H. S. Lee, H. H. Choi, D. H. Kim, S. G. Lee and K. Cho, *Adv. Funct. Mater.*, 2012, **22**, 267-281.

30 K. E. Strawhecker, S. K. Kumar, J. F. Douglas and A. Karim, *Macromolecules*, 2001, **34**, 4669-4672.

31 Y. S. Kim, Y. Lee, J. K. Kim, E. O. Seo, E. W. Lee, W. Lee, S. H. Han and S. H. Lee, *Curr. Appl. Phys.*, 2010, **10**, 985-989.

32 M. Santin, A. Motta, G. Freddi and M. Cannas, *J. Biomed. Mater. Res.*, 1999, **46**, 382-389.

33 X. Hu, D. Kaplan and P. Cebe, *Macromolecules*, 2006, **39**, 6161-6170.

34 I. C. Um, H. Y. Kweon, K. G. Lee and Y. H. Park, *Int. J. Biol. Macromol.*, 2003, **33**, 203-213.

35 H. J. Jin, J. Park, V. Karageorgiou, U. J. Kim, R. Valluzzi and D. L. Kaplan, *Adv. Funct. Mater.*, 2005, **15**, 1241-1247.

36 D. H. Kim, H. S. Lee, H. C. Yang, L. Yang and K. Cho, *Adv. Funct. Mater.*, 2008, **18**, 1363-1370.

37 W. H. Lee, S. G. Lee, Y. J. Kwark, D. R. Lee, S. Lee and J. H. Cho, *ACS Appl. Mater. Inter.*, 2014, **6**, 22807-22814.

38 D. K. Hwang, M. S. Oh, J. M. Hwang, J. H. Kim and S. Im, *Appl. Phys. Lett.*, 2008, **92**, 013304-013306.

39 D. K. Hwang, K. Lee, J. H. Kim, S. Im, J. H. Park and E. Kim, *Appl. Phys. Lett.*, 2006, **89**, 093507-093509.

40 T. Jung, A. Dodabalapur, R. Wenz and S. Mohapatra, *Appl. Phys. Lett.*, 2005, **87**, 182109-182111.

41 M. H. Yoon, C. Kim, A. Facchetti and T. J. Marks, *J. Am. Chem. Soc.*, 2006, **128**, 12851-12869.

42 G. Gu, M. G. Kane, J. E. Doty and A. H. Firester, *Appl. Phys. Lett.,* 2005**, 87 (24)**, 243512-243514.

43 W. H. Lee, H. Choi, D. H. Kim and K. Cho, *Adv. Mater.,* 2014**, 26**, 1660-1680.

44 H. Sirringhaus, *Adv. Mater.,* 2009**, 21**, 3859-3873.

45 P. A. Bobbert, A. Sharma, S. G. J. Mathijssen, M. Kemerink and D. M. de Leeuw, *Adv. Mater.,* 2012**, 24**, 1146-1158.

RSC Advances Accepted Manuscript